

# Charge density wave transport in submicron antidot arrays in $\text{NbSe}_3$

Yu. I. Latyshev<sup>1,2</sup>, B. Pannetier<sup>1</sup>, P. Monceau<sup>1</sup>

<sup>1</sup>Centre de Recherches sur les Très Basses Températures, associé à l'Université Joseph Fourier, CNRS, BP 166, 38042 Grenoble-Cedex 9, France.

<sup>2</sup>Institute of Radioengineering and Electronics,  
Russian Academy of Sciences, Mokhovaya 11,  
103907 Moscow, Russia

We demonstrate for the first time that a periodic array of submicrometer holes (antidots) can be patterned into thin single  $\text{NbSe}_3$  crystals. We report on the study of charge density wave (CDW) transport of the network of mesoscopic units between antidots. Size of the elementary unit can be as small as 0.5  $\mu\text{m}$  along the chain axis and 0.2  $\mu\text{m}$ –0.3  $\mu\text{m}$  in cross section. We observe size effects for Ohmic residual resistance and in CDW transport current-voltage characteristics in submicronic networks.

PACS index category: 71.45.Lr, 73.20.Mf, 73.23.Ps

## I. INTRODUCTION

There is a considerable interest in the study of mesoscopic CDW structures the characteristic size of which is comparable with the coherence length for the phase or the amplitude of the CDW order parameter. From these studies it is expected to obtain new information about the intrinsic coherence of the CDW conduction<sup>1</sup>. Recent experimental and theoretical investigations have demonstrated the possibility of the observation of quantum interference effects in heterostructures<sup>2,3</sup> and nanostructures<sup>4</sup> in CDW materials. Progress in mesoscopic CDW studies is foreseeable with the recent development of epitaxial thin film technology<sup>5</sup> combined with electron lithography technique. In the present publication, we report on CDW transport in submicron structures patterned on thin single crystal of the CDW quasi one-dimensional (Q1D) compound  $\text{NbSe}_3$ .

## II. EXPERIMENTAL

The idea of the experiment was to carry out the realization of a mesoscopic structure in which CDW motion is localized in an array of small cells with a submicron size, each cell being electrically connected to the neighbouring ones by transverse (to the chains) conduction. We show in Fig. 1 a schematic example of such a structure. The chain direction of Q1D  $\text{NbSe}_3$  is along x axis. A triangular lattice of holes (antidots) is made in such a way that the projection of holes along the y direction overlaps, that provides small units of CDW conduction between neighbouring holes. The individual cell is shown in Fig. 1 as a shaded rectangle.

We selected the most perfect thin  $\text{NbSe}_3$  crystals with a thickness,  $d$ , less than 1  $\mu\text{m}$  and a relatively large width  $w$  ( $w > 20 \mu\text{m}$ ). The width is along the c crystallographic axis. The  $\text{NbSe}_3$  crystals were first glued onto a silicon or sapphire substrate using a fluid resist. After baking 10 minutes at 130 °C the residues of resist were removed by a soft oxygen plasma etching. The crystal were then thinned using  $\text{SF}_6$  reactive ion etching down to about 0.5  $\mu\text{m}$  thickness. A 25 nm thin layer of silicon is then deposited by e-beam evaporation to protect the surface of the crystal and insure charge evacuation from the sapphire substrate during the subsequent e-beam lithography.

The desired holes have high aspect ratio: the hole size is 0.4–0.6  $\mu\text{m}$ , wall thickness is about 0.2  $\mu\text{m}$  and crystal thickness is 0.5  $\mu\text{m}$ . One therefore needs a sharp metallic mask. We first spin on a PMMA layer of nominal thickness 0.5  $\mu\text{m}$  and bake it 160 °C during 10 minutes. This PMMA layer is then patterned by direct writing with the electron beam of a scanning electron microscope and developed. We prepare a 50 nm aluminum mask by angle evaporation onto the surface of the patterned PMMA layer.

The etching of  $\text{NbSe}_3$  is then achieved in a  $\text{SF}_6$  plasma with the aluminum film. We have checked optically that for most of the samples the depth of etching coincides with the thickness of the crystal itself. We then remove the aluminum mask by wet etching and the PMMA layer in an oxygen plasma.

We have measured two  $\text{NbSe}_3$  samples with triangular lattice of holes, keeping nearly the same the ratio between the antidot lattice periodicity and the average diameter of the holes. The scanning electron micrographs in the patterned parts are shown in Fig. 2. The triangular lattice of antidots for sample # 1 (deposited on a silicon substrate) as shown in Fig. 2a has a periodicity  $S_b = 3 \mu\text{m}$  along the b axis and  $S_c = 3.7 \mu\text{m}$  along the c axis. The hole cross section nearly circular is 1.4  $\mu\text{m}$  x 1.5  $\mu\text{m}$ . For sample # 2 (deposited on a sapphire substrate) the periodicity of the lattice

of antidots is  $S_b = S_c = 0.6 \text{ m}$  with a rectangular hole cross section with  $D_b = 0.3 \text{ m}$  along the b axis and  $D_c = 0.4 \text{ m}$  along the c axis (see Fig. 2b).

Four gold contact pads are then patterned in a second e-beam lithographic step using lift-off technique. External leads are attached to the gold strips using indium contacts. The contact geometry is chosen to allow measurements on adjacent patterned and non-patterned zones (typical length:  $100 \text{ m}$ ) of the same crystal as drawn in Fig. 3. The microhole structure covers the whole width of the crystal.

The electrical resistance and the differential current voltage characteristics were measured with a  $40 \text{ Hz}$  phase sensitive bridge using the inner probes 1-2 and 3-4 as voltage probes to compare the properties of the patterned and non-patterned segments.

All the sample parameters are indicated in Table 1.

### III. RESULTS

The processing treatment yields some changes in the properties of the  $\text{NbSe}_3$  samples. In Fig. 4a we show the temperature dependence of a  $\text{NbSe}_3$  sample before processing and after processing (essentially the baking of the PMMA layer at  $160^\circ\text{C}$ ). The consequences of processing are an increase of both Peierls transition temperatures ( $T_{P_1} = 145 \text{ K}$  and  $T_{P_2} = 59 \text{ K}$  for pure  $\text{NbSe}_3$  crystals), an increase of the resistance at both maxima in the  $R(T)$  dependence and a larger residual resistance at low temperatures. However the sample still conserves all the properties of a relatively good quality  $\text{NbSe}_3$  crystal. After processing but without patterning the resistance ratio  $R(290 \text{ K})/R(4.2 \text{ K})$  is in range of 25-40 and the threshold electric field for CDW depinning at  $50 \text{ K}$  is  $E_T = 100 \text{ mV/cm}$ .

Patterning the antidot array strongly affects the resistance of the  $\text{NbSe}_3$  sample. In what follows each  $\text{NbSe}_3$  sample measured will have been processed on its total surface but only a part is patterned (see Fig. 3). The sheet resistance of the patterned part increases considerably, for instance by a factor 6.5 at room temperature for sample # 2; however the Peierls transition temperatures are not changed with respect to the unpatterned part as shown in Fig. 4b. The effect of patterning is clearly seen in the temperature dependence of the ratio between the resistance of the patterned part and the resistance of the unpatterned part. Prominent features appear near both Peierls transition temperatures and at low temperatures below  $50 \text{ K}$ . The decrease of the resistance of the patterned part below  $50 \text{ K}$  is largely suppressed for sample # 2 with the shorter antidot lattice periodicity. Thus, the resistance ratio between room temperature and helium temperature is 10 for sample # 1 and 4.8 for sample # 2 (to be compared to 25-40 for the unpatterned zone).

Fig. 5 shows the variation of the differential resistance  $\frac{dV}{dI}$  as a function of the applied current for both non-patterned (Fig. 5a) and patterned (Fig. 5b) parts of sample # 2. CDW motion occurs above a threshold electric field  $E_T$  defined as  $E_T = \frac{V_T}{L} = \frac{RI_T}{L}$  with  $R$  the Ohmic resistance,  $L$  the distance between electrodes and  $I_T$  the critical current at which non linearity in the  $(I-V)$  characteristics appears. It can be noted that  $I_T$  for the lower CDW is nearly identical for the patterned and unpatterned parts as shown in Fig. 6.

### IV. ANALYSIS AND DISCUSSION

We will now describe a simple model in order to explain the properties of submicronic structures patterned on a single  $\text{NbSe}_3$  crystal. We consider that: 1) transport along chains occurs only in the short cells located between neighbouring holes (shaded part in Fig. 1) and 2) transport from one cell to the adjacent one requires charge motion perpendicularly to the chains. One can imagine an equivalent scheme which consists in an electrical network with two types of resistances: one,  $R$ , for transport along the chains, the other,  $r$ , for transport across the chains as drawn in Fig. 7.

#### A. Ohmic behaviour

The ratio between the sheet resistance of the patterned part,  $R$ , and that of the unpatterned one,  $R_0$ ,  $G = \frac{R}{R_0}$  can be expressed as a linear function of  $r/R$ , which is proportional to the resistivity anisotropy  $\rho_c/\rho_b$  ( $\rho_c$ : resistivity along the width of the sample,  $\rho_b$ : resistivity along the chain axis). Thus,  $G = A + B(\rho_c/\rho_b)$  where  $A$  and  $B$  are coefficients depending on the geometry of the network. In the case where  $A = 1$  and  $\rho_c/\rho_b = 1$  which is appropriate in the present case, one can write:

$$G = B \frac{c}{b} \quad (1)$$

For sample # 2, we find  $G = 6.5$  at room temperature. Using the value of  $\rho_c = \rho_b = 15$  m measured at room temperature in  $\text{NbSe}_3$ <sup>6</sup>, one obtains  $B = 0.43$ . The justification for the validity of our conduction model is shown in Fig. 8 where we have drawn the temperature dependence of  $\frac{G(T)}{B}$  with  $B = 0.43$  and that of the resistivity anisotropy  $\rho_c = \rho_b$  measured in<sup>6</sup> using the Montgomery technique. A good agreement between the temperature dependence of both quantities is found in the full temperature range above  $T \approx 55$  K (remember that  $T_{p1}$  and  $T_{p2}$  are larger in our processed samples). At lower temperatures, Eq. 1 is invalid, because the additional contribution to the resistance due to the patterned structure. We consider that the origin of this additional contribution comes from the additional scattering in the mesoscopic units, when the mean free path,  $\lambda$ , becomes comparable at low temperatures to the length of the unit along the chains. Using the data from<sup>7</sup> for the carrier mobility along chains, we estimate that  $\lambda$  is  $0.3$  m at  $T = 40$  K. Below this temperature, the increase of  $\lambda$  becomes limited by the antidot periodicity. That can explain the decrease of the residual resistance ratio from 10 (sample # 1) to 4.8 (sample # 2) when the antidot lattice periodicity along the b axis is reduced from  $S_b = 3$  m (sample # 1) to  $0.6$  m (sample # 2).

### B. Threshold field for CDW depinning

We consider now the CDW depinning in a network structure. The threshold we have defined in part 3 corresponds to a value averaged over the whole structure. Let it to be noted as:  $\langle E_T \rangle = \frac{R}{L} \langle I_T \rangle$ .

However, it is also possible to define a local threshold field, noted as  $E_t$ , in an elementary cell: the shaded rectangle for the patterned part as shown in Fig. 1 with dimensions  $\lambda$  along the b axis and  $\lambda^0$  along the c axis. If the elementary cell extends half the distance between units along b axis as represented in Fig. 1, then  $\lambda = S_b$  and  $\lambda^0 = S_c - D_c$ . For the unpatterned part, the elementary cell is larger with dimensions  $S_b$  along the b axis and  $S_c$  along the c axis.  $E_t$  is connected with the local current  $I_t$ , along the chains in that elementary cell such as  $I_t = \rho_b E_t S$  where  $\rho_b$  is the linear conductivity along the chains and  $S$  the cross section of the sample. The ratio between  $E_t$  in the patterned part and the threshold field of the non-patterned part, that one notes as  $E_t^0$ , can be expressed as follows:

$$\frac{E_t}{E_t^0} = \frac{I_t}{I_t^0} \frac{\lambda^0}{\lambda} \frac{S_c}{S_c - D_c}$$

One then makes the reasonable assumption that the local  $\frac{E_t}{E_t^0}$  is the same than the average value for the whole sample  $\langle \frac{E_t}{E_t^0} \rangle$ .

For sample # 2 we have shown the temperature dependence of  $\langle I_T \rangle$  and  $\langle I_T^0 \rangle$  in Fig. 6. The temperature variation of  $\frac{\langle I_T \rangle}{\langle I_T^0 \rangle}$  for sample # 1 and # 2 are drawn in Fig. 9.

For sample # 1, with a larger cell size ( $D_c = 1.4$  m,  $D_b = 1.5$  m), we find that  $\langle I_T \rangle = \langle I_T^0 \rangle \approx 0.7$  with no significant temperature dependence. For this sample,  $\frac{S_c}{S_c - D_c} = 1.6$ ; one neglects any size effect for  $\rho_b$  such as  $\rho_b = \rho_b^0 = 1$ . Then  $E_t = E_t^0 \approx 1.1$  not far from the value of 1.

For sample # 2, with  $D_b = 0.3$  m and  $D_c = 0.4$  m, we measure  $\langle I_T \rangle = \langle I_T^0 \rangle = 1.2$  (Fig. 9). With  $\frac{S_c}{S_c - D_c} = 3$ , one gets  $E_t = E_t^0 \approx 4$ , demonstrating that there is a well pronounced size effect for the local  $E_t$  in a cell with submicron size. Similar size effects have been previously observed in  $\text{TaS}_3$  single crystals with a very small cross section<sup>8</sup> and a short length<sup>9</sup>.

### C. Current conversion

One of the aims of our study is the conduction due to CDW motion in a submicron unit. The process of conversion of the normal carrier current into a CDW current is still not well understood. In several theoretical models the conversion process is accompanied by auto-localization of carriers<sup>10</sup>, formation of phase-slippage centers<sup>11</sup>, dynamical amplitude solitons<sup>12</sup>, tunneling between solitons under the barrier<sup>13</sup>.

Phase slippage at current injection electrodes has resulted from experiments in which the variation of the threshold voltage was studied as a function of the distance between electrodes. It was found<sup>14</sup>, that :

$$V_T = E_p L + V_0$$

The first term corresponds to the bulk pinning due to impurities and the extra term  $V_0$  was interpreted as the potential necessary for the nucleation of a CDW dislocation loop for conversion of normal current into the CDW

condensate. Typically for NbSe<sub>3</sub>  $V_0$  is in the range of 0.2-0.5 mV at  $T = 40$  K<sup>14</sup>.

One can estimate the threshold voltage in our elementary cell of the patterned zone. The local critical current is the total critical current  $hI_T$  divided by the number of channels along  $c$  axis. The resistance of the elementary cell can be calculated according to its dimensions and the conductivity at the given temperature. Thus, one estimates that at 40-50 K, the threshold voltage in the elementary cell is in the range of 50-100  $\mu$ V, much less than  $V_0$ . One is led to conclude that in our network geometry with submicronic dimensions where the current is fed to the elementary cell without any interface with a normal metal, there is no vortex dislocation loop generated.

The other models<sup>10;12;13</sup> estimate the conversion length,  $L_{conv}$ , to be of the order of  $h v_F = \Delta$  (  $\Delta$ : the CDW gap). An estimate of  $L_{conv}$  for NbSe<sub>3</sub> is 20 nm. One can expect to determine a value of the conversion length from experiments on short samples with a length comparable with  $L_{conv}$ . In such a short sample only a part of the length of the sample,  $\sim 2L_{conv}$ , contributes to the non-linear conduction. A comparison with a macroscopic sample with the same thickness and the same ratio length/width can be made. It is then expected that in small samples the maximum contribution to the non-linear conduction will be at least  $\frac{2L_{conv}}{L}$  smaller.

We have measured the non-linear properties in the current regime where the CDW conduction saturates i.e.  $I > 10hI_T$  for both patterned and unpatterned parts of sample # 2. We obtain that the CDW conductivity in an individual cell,  $\sigma_{CDW}$ , is always smaller in the patterned part of the sample with respect to the value in the non-patterned part of the same sample,  $\sigma_{CDW}^0$ . Fig. 10a shows the temperature dependence of  $\sigma_{CDW} = \frac{\sigma_{CDW}}{\sigma_{CDW}^0}$ . Making the suggestion that this ratio is a measurement of  $\frac{2L_{conv}}{L}$ , one can estimate  $L_{conv}$  as equal to  $\frac{L}{2}$ . That yields a value of  $L_{conv}$  of 10-20 nm the temperature variation of which is drawn in Fig. 10b. This estimate of  $L_{conv}$  is in reasonable agreement with the theoretical calculations<sup>10;12;13</sup>.

## V. CONCLUSIONS

We have realized submicron antidot arrays in thin single NbSe<sub>3</sub> crystals. The comparison between the transport properties respectively in the patterned and unpatterned parts of the crystal reveals specific features of Ohmic conduction and CDW transport in submicron units.

## VI. ACKNOWLEDGEMENTS

The work was partly supported by the Russian State Program "Physics of Solid State Nanostructures" (project Nr 97.1052) and by CNRS through the PICS Nr. 153.

---

<sup>1</sup> For reviews in charge density wave properties in quasi-one-dimensional conductors: "Electronic Properties of Inorganic Quasi-One-Dimensional Compounds", Parts 1 and 2, P. Monceau ed. (D. Reidel, Boston 1985); G. G. Lonzarich, Rev. Mod. Phys. 60 (1988) 1129.

<sup>2</sup> A. A. Sinchenko et al., Zh. Eksp. Teor. Fiz. (1996).

<sup>3</sup> B. Rejaei and G. E. W. Bauer, Phys. Rev. B 54 (1996) 8487.

<sup>4</sup> Yu. I. Latyshev, O. Laborde, P. Monceau and S. Klumpp, Phys. Rev. Lett. 78 (1997) 919.

<sup>5</sup> H. S. J. van der Zant, O. C. M. Antel, C. Dekker, J. E. M. Ooiij and C. Traeholt, Appl. Phys. Lett. 68 (1996) 3823.

<sup>6</sup> N. P. Ong and J. W. Brill, Phys. Rev. B 18 (1978) 5265.

<sup>7</sup> N. P. Ong, Phys. Rev. B 18 (1978) 5272.

<sup>8</sup> D. V. Borodin, S. V. Zaitsev-Zotov, F. Ya. Nad', Zh. Eksp. Teor. Fiz. 93 (1987) 1394.

<sup>9</sup> S. V. Zaitsev-Zotov, V. Ya. Pokrovskii and J. C. Gill, J. Phys. I France 2 (1992) 111.

<sup>10</sup> S. A. Brazovskii, Zh. Eksp. Teor. Fiz. 78 (1980) 677.

<sup>11</sup> L. P. Gor'kov, Zh. Eksp. Teor. Fiz. 86 (1984) 1818.

<sup>12</sup> S. N. Artemenko, A. F. Volkov, A. N. Kuglov, Zh. Eksp. Teor. Fiz. 91 (1986) 1536.

<sup>13</sup> I. V. Krive et al., Pis'ma Zh. Eksp. Teor. Fiz. 46 (1987) 99.

<sup>14</sup> P. Monceau, M. Renard, J. Richard and M. C. Saint-Lager, Physica 143B (1986) 64.

Table of sample parameters

Sample	Hole parameters		Spacing		Patterned zone		Unpatterned zone	
	$D_b$	$D_c$	$S_b$	$S_c$	Length	Width	Length	Width
# 1	1.5	1.4	3.0	3.7	80	130	540	130
# 2	0.3	0.4	0.6	0.6	70	22	620	22

Table gives the dimension of the individual hole and of the periodicity of the antidot array (see Fig. 1) for sample # 1 and # 2. Dimensions of the samples are also indicated.

Figures

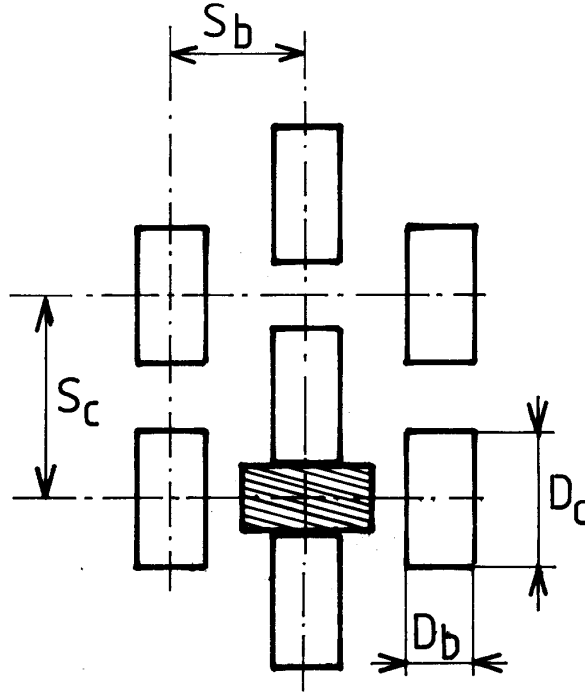
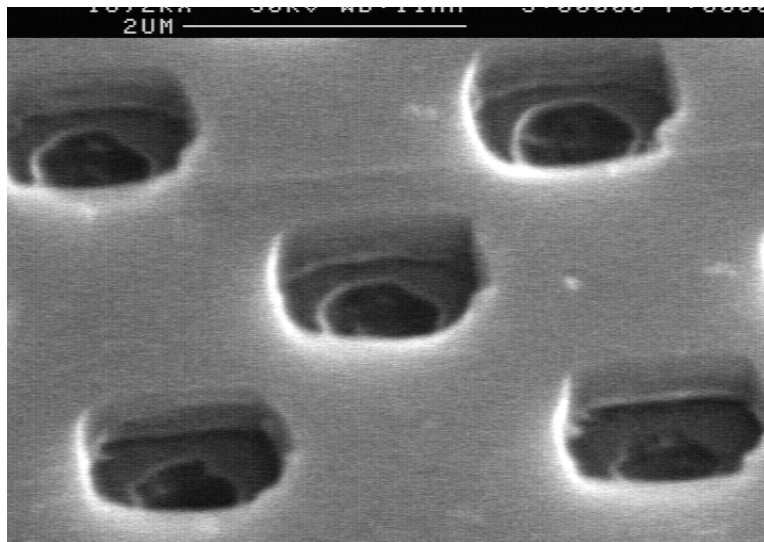
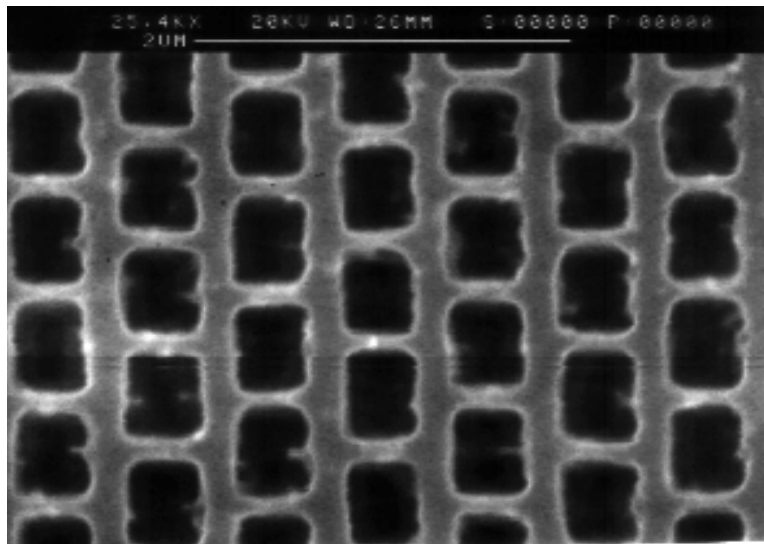


FIG. 1. Schematic picture of the structure with a triangle lattice of holes (antidots). The chain axis is along the X-direction. The projections of holes along the Y-direction overlap in order to block CDW motion in a cell between neighboring holes. Elementary CDW conducting unit is shown as the shaded rectangle



- a -



- b -

FIG .2. Scanning electron micrographs of the patterned parts of  $\text{NbSe}_3$ . a) sample # 1 on a silicon substrate, b) sample # 2 on a sapphire substrate.

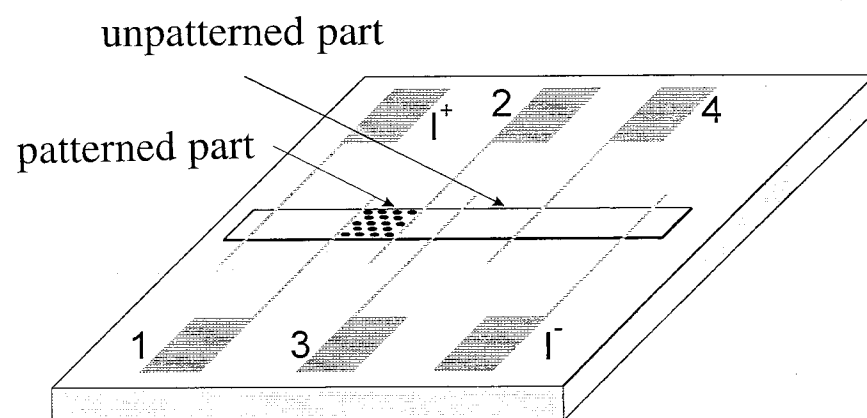


FIG. 3. The geometry of the experiment.

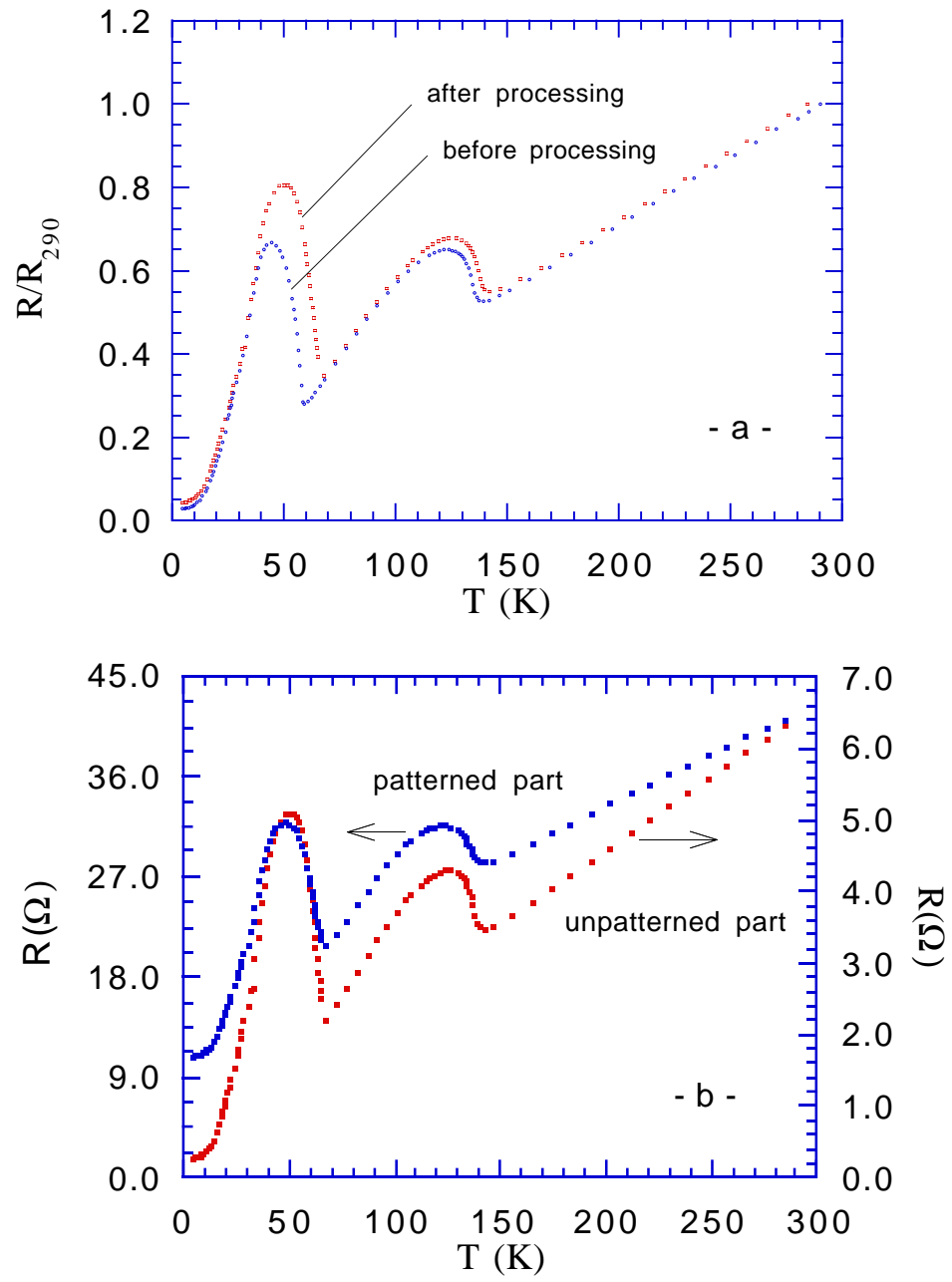


FIG. 4. Temperature dependences of the resistance of NbSe<sub>3</sub> (sample # 2) a) before and after processing (baking the PMMA layer at 160 °C), b) of the patterned and unpatterned part after processing.



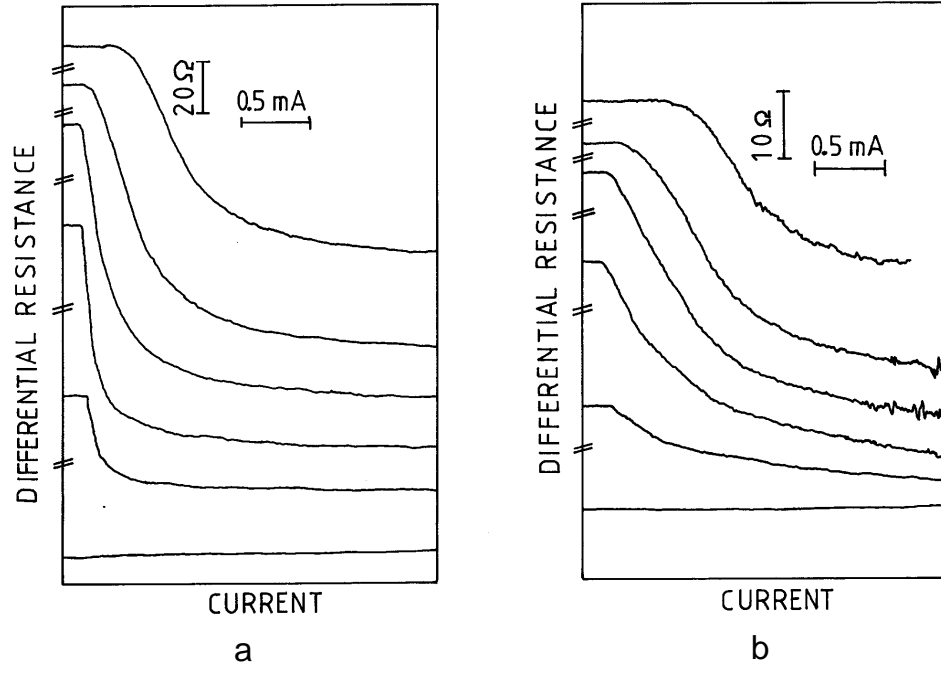


FIG . 5. Variation of the differential resistance  $\frac{dV}{dI}$ , as a function of current,  $I$ , for the patterned and the non-patterned parts of NbSe<sub>3</sub> (sample # 2). The temperatures from top to bottom are as follows : 38.3 K, 42.1, 49.8, 56.9, 62.7, 67.7 K. The corresponding linear resistances (in  $\Omega$ ) are as follows : 105, 106, 118, 107, 87, 76, (for the patterned part) and 118, 141, 151, 139, 98, 66 (for the non-patterned part).

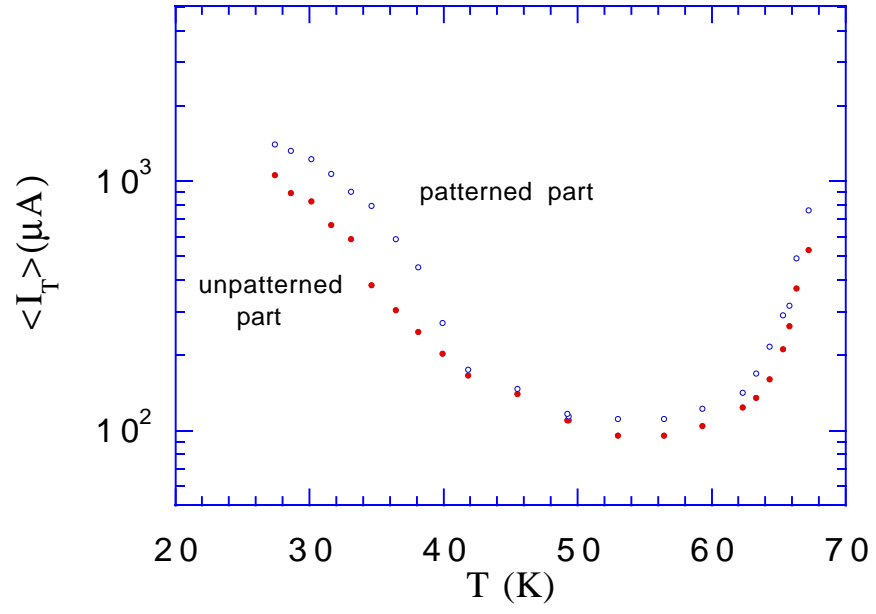


FIG . 6. Temperature dependences of the average threshold current  $\langle I_T \rangle$  for initiating the CDW conduction in NbSe<sub>3</sub> (sample # 2).

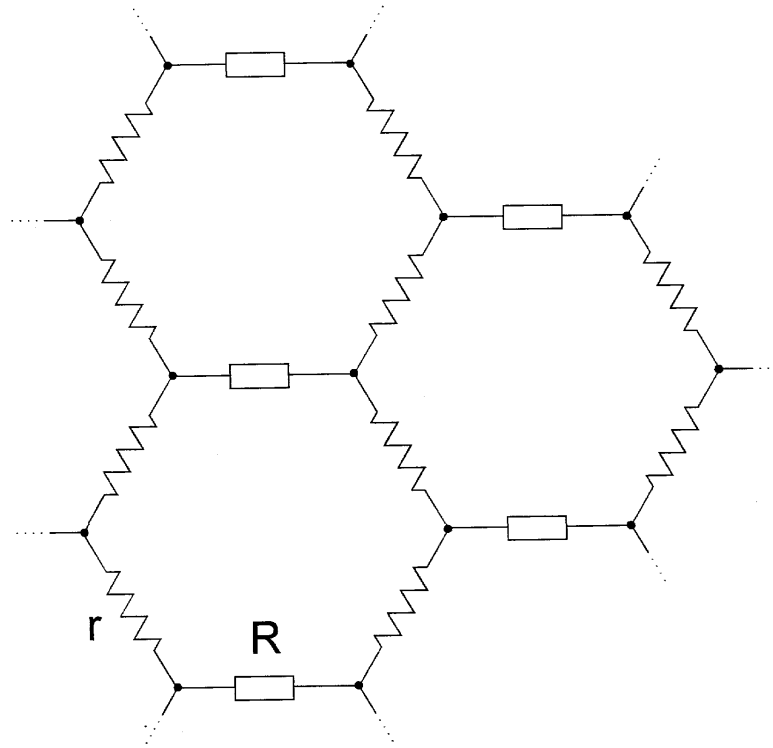


FIG . 7. The equivalent scheme of the patterned part.

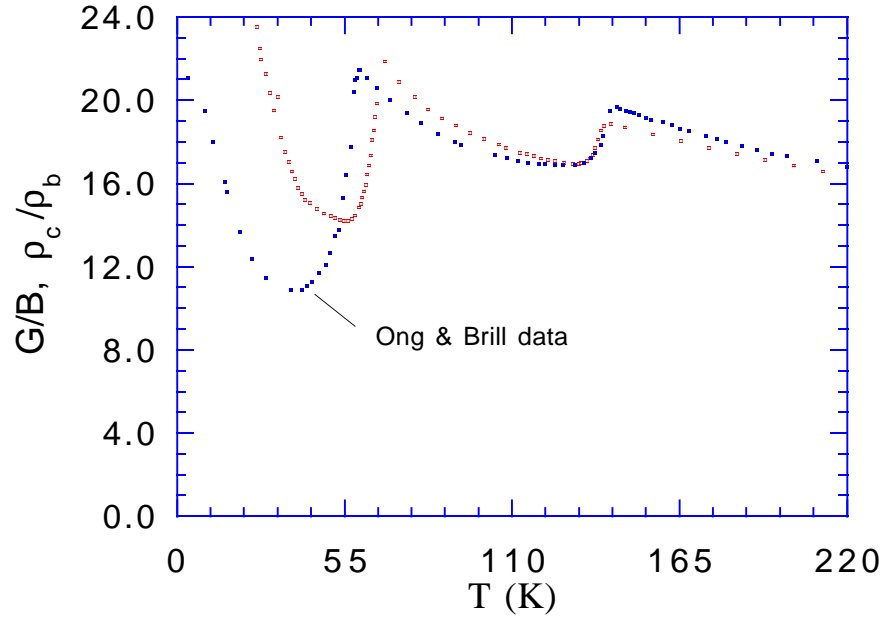


FIG .8. Temperature dependences of the normalized sheet resistance ratio of the patterned to the non-patterned parts,  $G/B$ , for sample # 2 (full squares) and the anisotropy ratio  $\rho_c/\rho_b$  measured by Montgomery technique (empty squares) from Ref.5. The factor  $B=0.43$  normalizes both quantities at the same value at room temperature.

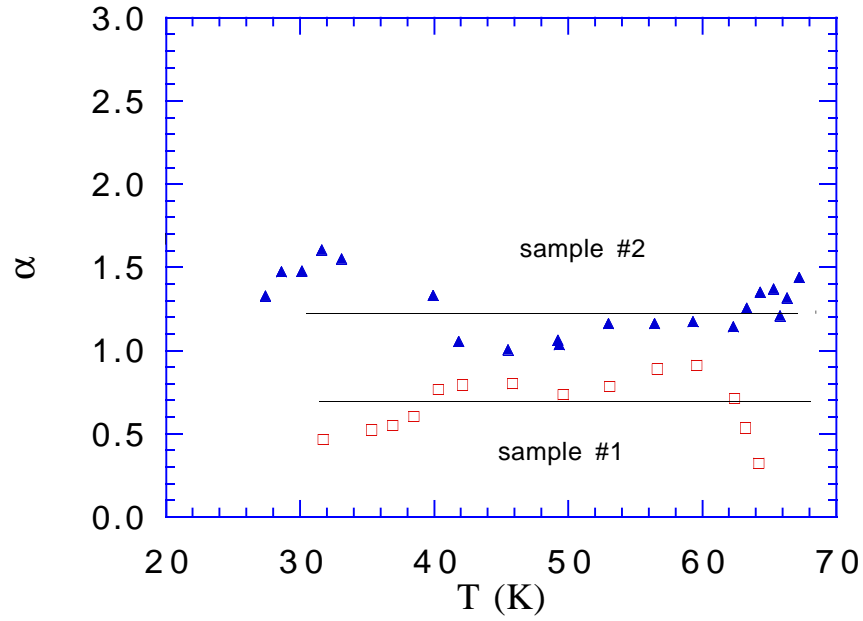


FIG .9. Temperature dependence of the ratio,  $\alpha$ , between average threshold current  $\langle I_T \rangle$  and  $I_T^0$  for the patterned and unpatterned parts of  $\text{NbSe}_3$  (sample # 1 and # 2).

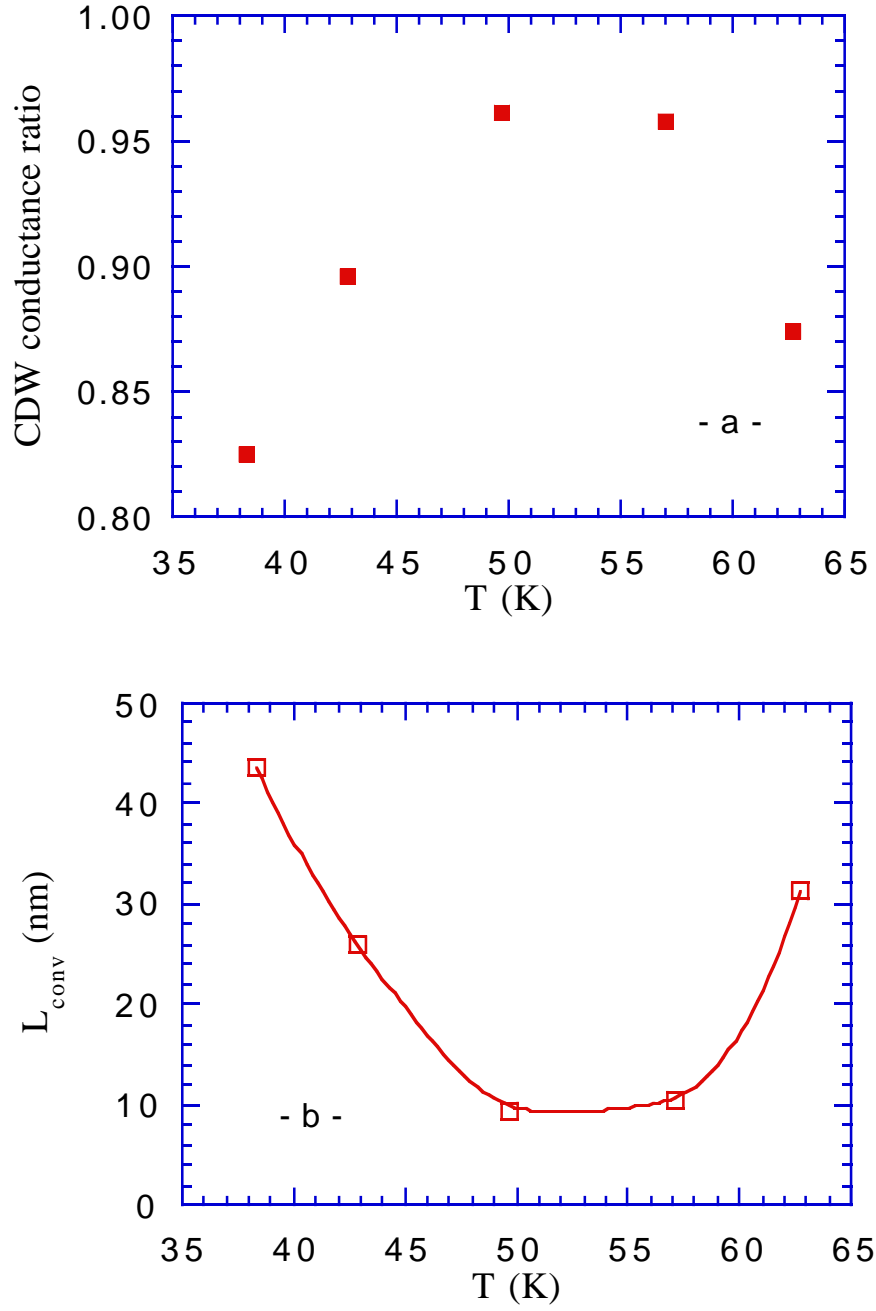


FIG .10. a) temperature dependence of the ratio of the CDW conduction in the submicron unit (shaded rectangle in Fig.1) and in the equivalent bulk part for applied current 10 times the average threshold value for  $\text{NbSe}_3$  (sample # 2); b) temperature dependence of the conversion length  $L_{\text{conv}}$  for normal carriers into CDW current (sample # 2). For the procedure to extract  $L_{\text{conv}}$  from data, see text.